# Enhancing the Luminous Efficiency of Ultraviolet Light Emitting Diodes By Adjusting the Al Composition of Pre-Well Superlattice

Yanli Wang, Peixian Li, Siyu Jiang, Xiaowei Zhou, Jinxing Wu, Wenkai Yue, and Yue Hao, *Senior Member, IEEE*

***Abstract*—The lower luminous efficiency is a critical issue for ultraviolet light-emitting diodes (UV-LEDs) owing to the poor carrier injection efficiency and high dislocation density. Here, we can improve the luminous efficiency in two avenues by adjusting the Al composition of the InGaN/$Al_xGa_{1-x}N$ pre-well superlattice. First, due to the strain-induced piezoelectric and intrinsic spontaneous polarization, a large number of electrons gather at the InGaN/$Al_xGa_{1-x}N$ interface, which improves the electron concentration of the pre-well superlattice and lowers the conduction band energy of the first quantum barrier layer (FQB), thus enhancing the electron injection efficiency. Second, the pre-well superlattice can act as a hole blocking layer to prevent holes from leaking into the n-type layer and confine them in the quantum well layer. As the Al composition increases, the hole blocking effect of the pre-well superlattice is strengthened. However, higher Al composition decreases the lattice quality, which makes it possible for carrier loss through defect-related non-radiative recombination. Finally, the output power of the samples with 5% Al composition in the pre-well superlattice is 5.9% and 102.5% higher than that of the samples with 3% and 7% Al composition, respectively.**

***Index Terms*—Ultraviolet light-emitting diodes, hole blocking layer, superlattice, APSYS.**

## I. Introduction

IN THE last few years, ultraviolet light-emitting diodes (UV-LEDs) have received a lot of attention for their wide applications [1]–[2]. However, the low luminous efficiency caused by the strong polarization induced poor carrier injection efficiency and mismatch induced high dislocation density limits their development, for which substantial efforts have been devoted [3]–[4]. One way to raise the luminous efficiency is to increase the carrier injection efficiency [5], which includes improving the hole concentration in the p-type layer and preventing electron leakage. In the III-nitride UVLEDs, high background carrier concentration and Mg activation energy result in low hole injection efficiency in the p-type injection layer [6]. For this reason, the three-dimensional hole gas (3DHG) and two-dimensional hole gas (2DHG) have been reported to enhance the hole concentration in the p-type layer [7]–[8]. And the hole blocking layer has also been demonstrated to confine holes in multiple quantum wells (MQWs) to facilitate hole injection [9]. It is well known that the polarization-induced electric field between the last quantum barrier layer (LQB) in MQWs and the p-type layer lowers the energy band at the interface, causing electrons to leak into the p-type, thereby participating in non-radiative recombination [10]. Various approaches, such as employing high Al composition AlGaN electron blocking layer (EBL) [11], graded EBL [12], insertion layer in EBL [13], and multi-quantum barriers EBL [14], have been put forward to cope with this problem. Besides, lowering the dislocation density is as well considered a working way to maximize luminous efficiency. For example, Using the patterned sapphire substrates (PSSs) technology [15]–[16], epitaxial lateral overgrown (ELOG) [17]–[18] and low-temperature deposited buffer layer [19] are capable of reducing the defect-related non-radiative recombination. In our previous work, double superlattices structure with 30-period Mg modulation-doped p-AlGaN/u-GaN superlattice p-type layer and 4-period p-AlGaN/p-GaN superlattice EBL, and double Al composition gradient last quantum barrier and p-type hole supply layer structure were proposed to improve the hole injection efficiency and suppress electron leakage, resulting in UV-LEDs with enhanced performance [20]–[21].

In this work, we mainly focus on how to improve the luminous efficiency by adjusting the Al composition of the InGaN/$Al_xGa_{1-x}N$ pre-well superlattice inserted between the n-type layer and MQWs. On the one hand, in the simulation analysis of the advanced physical model of semiconductor devices (APSYS), we distinctly observe that a large number of electrons clustered at the InGaN/$Al_xGa_{1-x}N$ heterojunction interface improve the electron concentration of the pre-well superlattice

Manuscript received April 16, 2021; revised May 26, 2021; accepted June 7, 2021. Date of publication June 10, 2021; date of current version September 16, 2021. This work was supported in part by the National Key R&D Program of China under Grant 2016YFB0400800, in part by the National Natural Science Foundation of China under Grant 61634005, in part by the Key R&D projects of Shaanxi Province under Grant 2018ZDCXL-GY-01-07, in part by the Key Research and Development program in Shaanxi Province under Grant 2018ZDCXL-GY-01-02-02, and in part by the WUHU Research Institute of Xidian University under Grant XWYCXY-012020007. *(Corresponding authors: Peixian Li; Xiaowei Zhou.)*

Yanli Wang, Peixian Li, Siyu Jiang, Xiaowei Zhou, Jinxing Wu, and Wenkai Yue are with the Wide Bandgap Semiconductor Technology Disciplines State Key Laboratory, School of Advanced Materials and Nanotechnology, Xidian University, Xi'an 710071, China (e-mail: ylwang055065@163.com; peixian_li@163.com; 18392101077@163.com; xwzhou@mail.xidian.edu.cn; jinxing_wu_xidian@163.com; yuewenkai888@gmail.com).

Yue Hao is with the Wide Bandgap Semiconductor Technology Disciplines State Key Laboratory, School of Microelectronics, Xidian University, Xi'an 710071, China (e-mail: yhao@xidian.edu.cn).

Digital Object Identifier 10.1109/JPHOT.2021.3088222

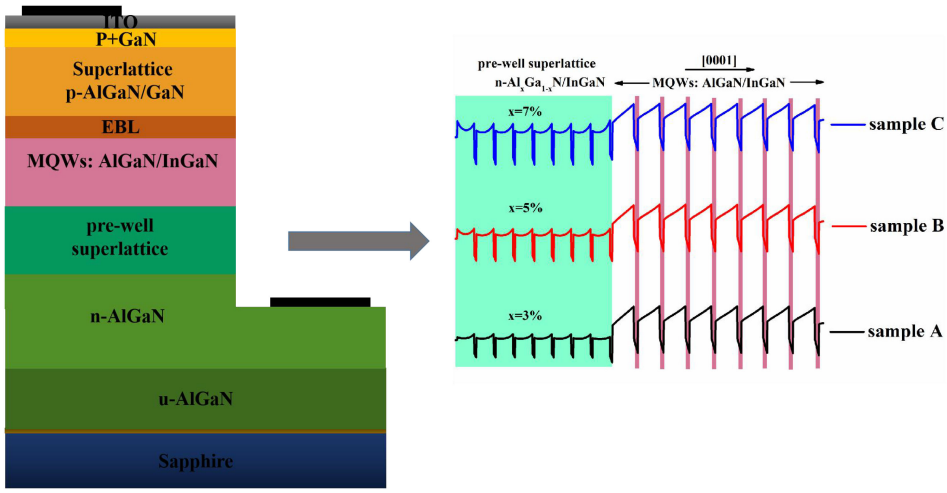


Fig. 1. Schematic structures of sample A, sample B and sample C.

and pull down the conduction band energy of the first quantum barrier layer (FQB) in MQWs to boost the electron injection efficiency. On the other hand, as a hole blocking layer, the pre-well superlattice contributes to prevent holes from leaking into the n-type layer and confine them in MQWs to participate in radiation recombination. Although the higher the Al composition, the greater the ability of the pre-well superlattice to improve carrier injection efficiency, which nevertheless also leads to a lower lattice quality. As a result, the enhanced optical output power is achieved when the Al composition of the pre-well superlattice is 5%. Compared to our previously reported samples with double superlattices and Si modulation-doped AlGaN/GaN, the optical power of UV-LEDs with the pre-well superlattice is increased by 62% and 72.7% at 120 mA, respectively.

## II. Experimental Details

As shown in Fig. 1, three InGaN/AlGaN UV-LEDs (sample A, sample B and sample C) are initiated on a c-plane (0001) 2-inch patterned sapphire substrate (PSS) by AIXTRON CRUIS I commercial metal-organic chemical vapor deposition system (MOCVD). Trimethyl-gallium, trimethyl-aluminium, trimethyl-indium and ammonia are used as source compounds. Hydrogen and nitrogen gas are carrier gas. First of all, a 25 nm AlN buffer layer is sputtered on PSS. The temperature and pressure of the reaction chamber are maintained at 1020°C and 400 mbar, respectively. A 4 $\mu$m unintentionally doped n-type $Al_{0.02}Ga_{0.98}N$ layer and a 3.3 $\mu$m Si-doped n-type $Al_{0.02}Ga_{0.98}N$ layer are grown sequentially. Then, we grow eight-pair the $In_{0.01}Ga_{0.99}N$/n-$Al_xGa_{1-x}N$ ($0.02<x<0.08$) pre-well superlattice, of which the well and barrier thickness is 1 nm and 8 nm, respectively. The x values in samples A, B and C are 3%, 5% and 7%, respectively. The ultraviolet photons are generated by MQWs with eight 2 nm $In_{0.01}Ga_{0.99}N$ wells embedded in nine 10 nm n-$Al_{0.08}Ga_{0.92}N$ barriers. During the growth process, the growing pressure of the well and barrier layer in the pre-well superlattice and MQWs are respectively 350 mbar and 200 mbar, and their temperatures are 750°C and 850°C, respectively. On the top of the MQWs, a 15 nm AlGaN-based p-EBL and 30-period 3 nm p-$Al_{0.16}Ga_{0.84}N$/2 nm u-GaN superlattice acting as the hole injection layer are grown at 150 mbar and 940°C, followed by the 10 nm thick heavily Mg-doped p+-type GaN layer. Lastly, the mesa structures with a size of 325 $\mu$m × 300 $\mu$m are obtained by conducting inductively coupled plasma etching.

TABLE I
The $\Phi_{1e}$, $\Phi_{1h}$, $\Phi_{2e}$ and $\Phi_{2h}$ Values for Three Samples

| Al | $\Phi_{1e}$ (meV) | $\Phi_{1h}$ (meV) | $\Phi_{2e}$ (meV) | $\Phi_{2h}$ (meV) |
|---|---|---|---|---|
| 3% | 91.53 | 138.82 | 243.37 | 277.43 |
| 5% | 89.2 | 166.31 | 242.73 | 277.38 |
| 7% | 85.23 | 191.7 | 241.6 | 277.22 |

The energy band profiles, carrier concentration, radiation coincidence rate and electron current are numerically investigated with a finite element approach by APSYS [22], which includes many sophisticated models such as tunnelling, heterojunctions, thermal analysis, and self-consistent quantum well models. The operating temperature, theoretical polarization charge, and Shockley-Read-Hall (SRH) recombination life are set to 300 K, 40%, and 20 ns, respectively.

## III. Results and Discussion

In order to investigate the effect of the Al composition of the pre-well superlattice on the energy band. Numerically computed band energy profiles for three samples at 120 mA are shown in Fig. 2(a-c). we define $\Phi_e$ and $\Phi_h$ as the potential difference between the conduction/valence band and the quasi-Fermi level. Table I presents the $\Phi_{1e}$, $\Phi_{1h}$, $\Phi_{2e}$ and $\Phi_{2h}$ values for three samples. As indicated in Fig. 2(a-c), the energy bands of the first quantum barrier (FQB) in MQWs are pulled down from∼91.53 meV for sample A to∼89.2 meV for sample B and then to∼85.23 meV for sample C. The lower $\Phi_{1e}$ allows more electrons into the quantum well to participate in radiative recombination. Moreover, as the Al composition increases, the bandgap of the potential barrier layer in the pre-well superlattice

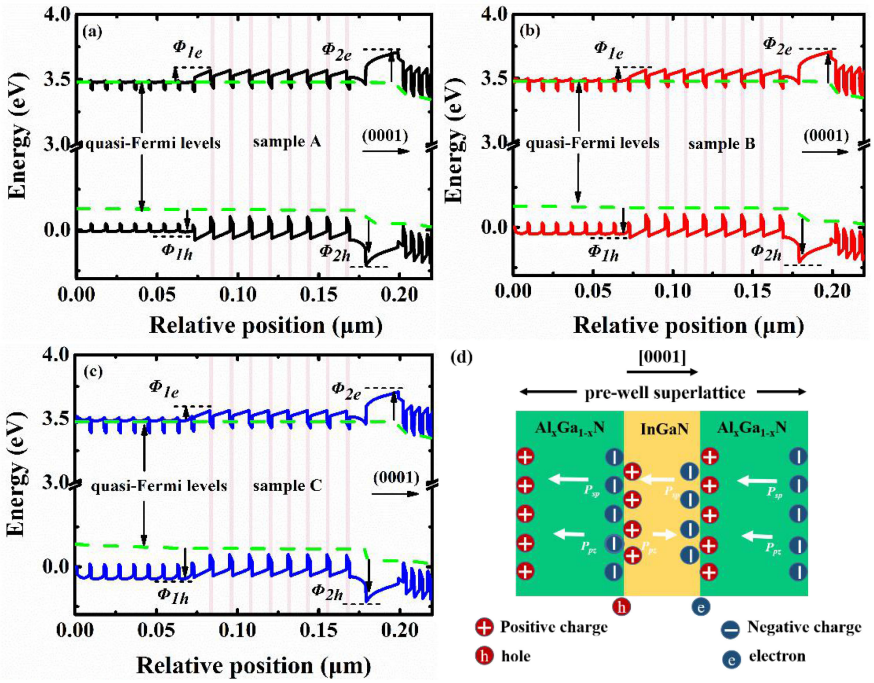


Fig. 2. Numerically computed band energy profiles (a): sample A, (b): sample B, (c): sample C at 120 mA, respectively. (d) The Schematic of the polarization induced charge distribution in the pre-well superlattice.

becomes larger, which leads to a gradual increase in $\Phi_{1h}$. The $\Phi_{1h}$ for three samples is 138.82 meV, 166.31 meV and 191.7 meV, respectively. The increased $\Phi_{1h}$ makes the pre-well superlattice act as a hole blocking layer (HBL), preventing holes from leaking to the n-type region. Then the charge distribution in the pre-well superlattice is illustrated in Fig. 2(d), where $P_{pz}$ and $P_{sp}$ represent the strain-induced piezoelectric and intrinsic spontaneous polarizations, respectively. Both the $Al_xGa_{1-x}N$ barrier and InGaN well layer endure intrinsic spontaneous polarization opposite to the growth direction. The piezoelectric polarization in the barrier layer is caused by the tensile strain from the n-$Al_{0.02}Ga_{0.98}N$ layer and has the same direction as the spontaneous polarization [23]. While the piezoelectric polarization in the well layer is driven by the stress-strain, whose direction is opposite to the spontaneous polarization. As a result, the barrier layer with the same polarization direction generates more charge than the well layer, which results in net positive charges at the InGaN/$Al_xGa_{1-x}N$ interface, thus inducing electrons to accumulate here. Accumulated electrons not only pull down the conduction band of the InGaN/FQB interface, as shown in Table I, which lowers $\Phi_{1e}$ and consequently improves electron injection efficiency, but also boost the electron concentration of the pre-well superlattice. In addition, the conduction band and valence band barrier heights ($\Phi_{2e}$ and $\Phi_{2h}$) of EBL are also calculated to study the influence of the pre-well superlattice on electron leakage and hole injection efficiency. As seen in Table I, there are only slight changes in $\Phi_{2e}$ and $\Phi_{2h}$ of the three samples.

The higher electron concentration observed among the pre-well superlattice and MQWs of sample C in Fig. 3(a) is presumably caused by the more net positive charges at the InGaN/$Al_xGa_{1-x}N$ interface due to the increased Al composition of the potential barrier layer. As mentioned in Fig. 2(d), on one hand, accumulated electrons at the InGaN/$Al_xGa_{1-x}N$ interface significantly raise the electron concentration of the pre-well superlattice. On the other hand, a reduced $\Phi_{1e}$ in the InGaN/FQB interface promotes electron injection efficiency and consequently lead to higher electron concentrations among MQWs. It is noteworthy that there is less hole concentration in the pre-well superlattice for sample C compared to samples A and B, in Fig. 3(b). This indicates that the pre-well superlattice acts as an HBL to prevent holes from leaking to the n-type region, which allows more holes to participate in radiative recombination in MQWs. Hence, the decreased and increased recombination rates appear in the pre-well superlattices and MQWs of sample C with higher Al composition, respectively, as displayed in Fig. 3(c). Moreover, the almost constant $\Phi_{2h}$ in Table I implies that the elevated hole concentration in MQWs is entirely attributable to the blocking effect of the pre-well superlattice. Although $\Phi_{2e}$ has slightly decreased, the leakage current of sample C in Fig. 3(d) is minimal, which may be due to abundant electrons being recombined in MQWs.

As demonstrated above, the enhanced performance of sample C can be ascribed to the increased Al composition in the $Al_xGa_{1-x}N$ barrier layer of the pre-well superlattice. Yet, epitaxial wafers are subject to numerous unavoidable factors in the growth process, resulting in discrepancies between experimental results and simulation analysis. In order to investigate the influence of Al composition on the performance of samples in specific experiments, the lattice quality, stress state and luminescence properties for three samples are displayed in the following diagrams.

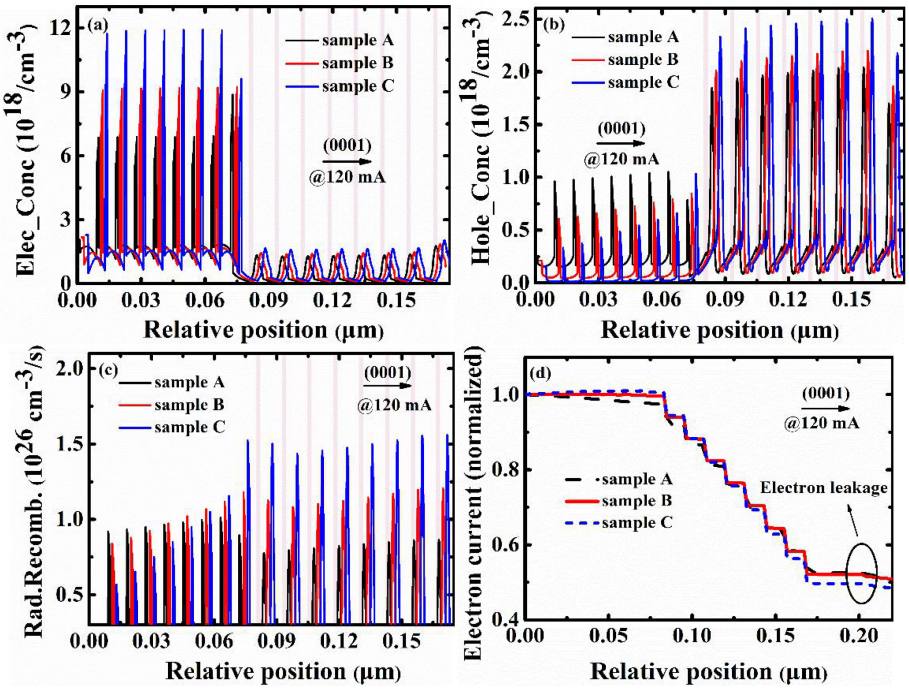


Fig. 3. (a) Electron concentration distributions, (b) hole concentration distributions, and (c) radiative recombination rate among pre-well superlattice and MQWs at 120mA. (d) Normalized electron current for three samples at 120mA.

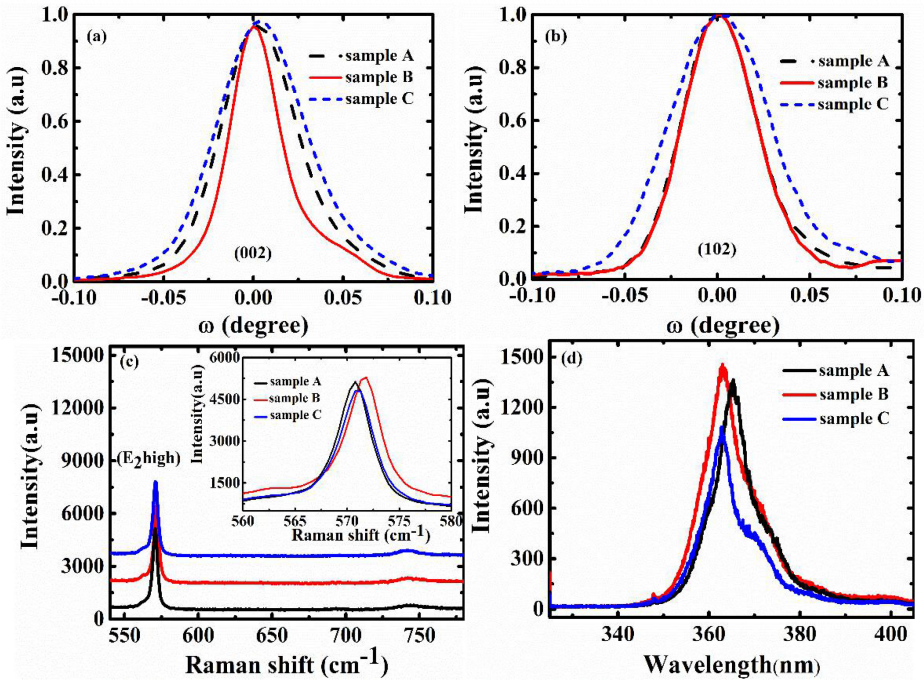


Fig. 4. HRXRD $\omega$-scans of the (a) symmetric (002) reflection and (b) asymmetric (102) reflection for three samples. (c) Raman spectra (inset is the magnification of the $E^2$(high) mode peaks). (d) PL spectrum at room temperature.

The HRXRD $\omega$-scan rocking curves of the (002)/(102) reflections for three samples are obtained by D8 DISCOVER in Fig. 4(a-b). The symmetric (002) rocking curve full width at half maximums (FWHM) of sample A, B and C are 181.4 arcsec, 120.4 arcsec and 210.2 arcsec, respectively, while the FWHMs of asymmetric (102) reflection are 171.1 arcsec, 169.9 arcsec and 230.5 arcsec, respectively. The FWHM of the crystal plane parallel to the c-axis can be used to characterize the screw dislocation density, while the edge dislocation leads to a broadening of the diffraction curve perpendicular to the c-axis. So the FWHM of the (002)/(102) reflections can characterize the screw/ edge dislocation density, respectively [24]. The formula

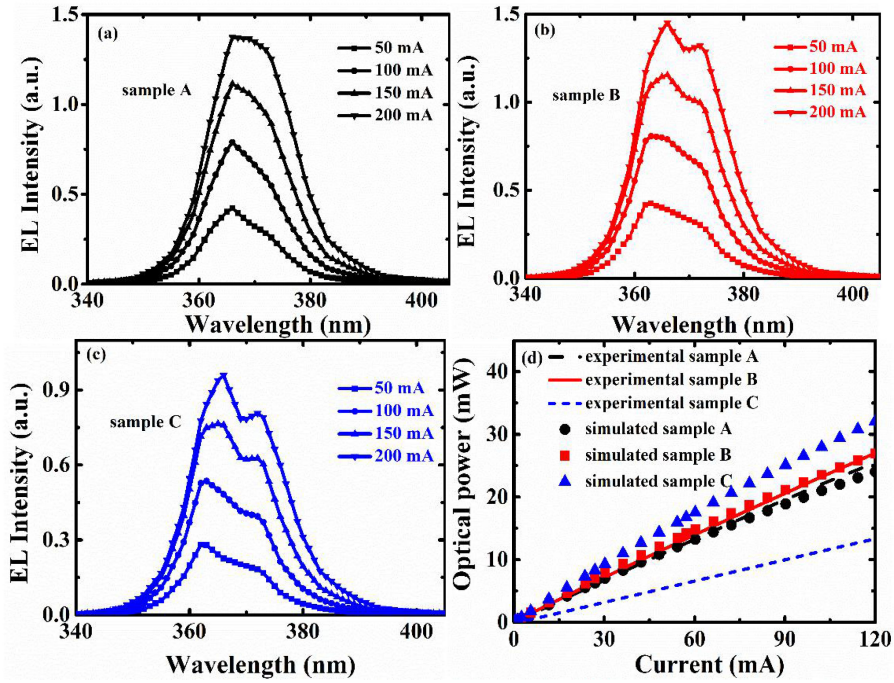


Fig. 5. (a-c) Electroluminescence spectra for three samples at 50 mA, 100 mA, 150 mA, 200 mA, 250 mA, and 300 mA respectively. (d) The experimental and simulated optical power of three samples.

for calculating dislocation density is as follows [25]:

$$\rho = \beta^2 / \left(4.36b^2\right) \quad (1)$$

where $\beta$ is the FWHM value of the HRXRD $\omega$-scan rocking curves, and $b$ represents the Burgers vector of the dislocation. The Burgers vectors of screw and edge dislocation are 0.5185 nm and 0.3189 nm, respectively. According to the HRXRD results, the screw (edge) dislocation density of sample B is $2.91\times10^7$ $cm^{-2}$ ($1.53\times10^8$ $cm^{-2}$), lower than sample A and C whose values are $6.61\times10^7$ $cm^{-2}$ ($1.56\times10^8$ $cm^{-2}$) and $8.88\times10^7$ $cm^{-2}$ ($2.82\times10^8 cm^{-2}$), respectively. This implies that sample B has the best lattice quality. To explore the stress states of three samples, the confocal Jobin Yvon LabRam HR800 is utilized to obtain the Raman spectra as shown in Fig. 4(c). There is a strong $E^2$(high) mode peak and a weak $E^1$(LO) peak in the Raman spectrum, located at approximately 568 $cm^{-1}$ and 750 $cm^{-1}$, respectively [26]. The $E^2$(high) mode peak is rather sensitive to the stress state, so its peak position can be used to reflect the stress state of materials [27]. As you can see from the inserted enlarged image, the mode peaks $E^2$(high) of samples A, B and C are positioned at 570.7 $cm^{-1}$, 571.9 $cm^{-1}$ and 571.3 $cm^{-1}$, larger than the strain-free 568 $cm^{-1}$, which means three samples are under compressive strain [28]. It is well known that dislocations can release stress and higher Al composition may introduce new stresses in the pre-well superlattice [29]. These two factors combine to give sample B a lower dislocation density and higher stress. And the higher intensity of sample B in the Raman spectra indicates the best lattice quality, which is in agreement with the HRXRD results. Apart from that, the PL spectrum of three samples is measured by the 325 nm laser diode at room temperature to investigate the luminescence performances. As illustrated in Fig. 4(d), the quantum well band edge peaks of three samples are located at 364.86 nm, 362.72 nm and 362.72 nm, respectively. While the weak peak (at~370 nm) is speculated to be caused by the pre-well superlattice. The observed blue shifts are caused by the compressive stress in MQWs as shown in Fig. 4(c). Furthermore, the luminescence intensity of sample B is stronger than that of samples A and C.

Electroluminescence (EL) spectra for three samples at different injection currents are obtained by Everfine ATA-500UV in Fig. 5(a-c). As the injection current increases from 50 mA to 200 mA, the peak wavelengths of samples A, B and C are all red-shifted by 2.3 nm, 1.6 nm and 1.9 nm respectively. However, Niu et al. reported that when the injection current increases, the peak wavelength of the devices should be blue shifted [30]. This is because the radiative recombination rate of the pre-well superlattice gradually increases with current, which broadens the El spectral curve and results in a red-shift of the peak wavelength. In sample A with low Al composition, the hole blocking effect is the smallest, so that a large number of holes flow into the pre-well superlattice to participate in radiative recombination. Therefore, sample A has no obvious peak wavelength of the pre-well superlattice and exhibits a maximum redshift. The EL intensity of MQWs in samples B and C, which have a higher hole blocking effect, is significantly stronger than that of the pre-well superlattice. And the redshift of sample B is lower than that of sample C with high dislocation density. Fig. 5(d) demonstrates the experimental and simulated optical power of three samples. It can be seen that the simulated results of samples A and B are in line with the experimental results. The high dislocation density makes it impossible to fit the experimental and simulation results for sample C. Compared to sample A and C, the optical power for sample B is enhanced by 5.9% and 102.5% at 120 mA, respectively. From the above discussion,

the enhanced performance originates from the promoted carrier injection efficiency (lower hole leakage and higher electron injection) and the decreased dislocation density.

## IV. Conclusion

In conclusion, we have proposed a method to promote luminous efficiency by adjusting the Al composition of the pre-well superlattice inserted between the n-type layer and MQWs. Simulation analysis shows that a large number of electrons accumulate at the InGaN/$Al_xGa_{1-x}N$ heterojunction interface due to polarization effects. Accumulated electrons pull down the energy bands of FQB from∼91.53 meV for sample A to∼89.2 meV for sample B and then to∼85.23 meV for sample C, which allows more electrons to be injected into MQWs to participate in radiative recombination. Moreover, the electron concentration in the pre-well superlattice is greatly increased, making it a viable method for obtaining high electron concentration in n-AlGaN with a high Al composition. As the hole blocking layer, the valence band barrier of the pre-well superlattice is improved from 138.82 meV to 191.7 meV with the Al composition increase, making MQWs more effective in confining the holes. However, the higher Al composition deteriorates the lattice quality. As a result, the enhanced optical output power is achieved when the Al composition of the pre-well superlattice is 5%.

## Acknowledgment

The authors wish to thank the anonymous reviewers for their valuable suggestions.

## References

[1] M. Hartensveld, B. Melanson, and J. Zhang, "Ultraviolet electrostatic field effect light-emitting diode," *IEEE Photon. J.*, vol. 12, no. 5, Oct. 2020, Art. no. 8200808.

[2] J. Zhang *et al.*, "The advantages of algan-based UV-LEDs inserted with a p-AlGaN layer between the EBL and active region," *IEEE Photon. J.*, vol. 5, no. 5, Oct. 2013, Art. no. 1600310.

[3] H. C. Tao, S. R. Xu, J. C. Zhang, P. X. Li, Z. Y. Lin, and Y. Hao, "Numerical investigation on the enhanced performance of N-polar algan-based ultraviolet light-emitting diodes with superlattice p-type doping," *IEEE Trans. Electron Devices*, vol. 66, no. 1, pp. 478–484, Jan. 2019.

[4] C. Huang, H. C. Zhang, and H. D Sun, "Ultraviolet optoelectronic devices based on AlGaN-SiC platform: Towards monolithic photonics integration system," *Nano Energy*, vol. 77, Nov. 2020, Art. no. 105149.

[5] Y. Li *et al.*, "Advantages of algan-based 310-nm UV light-emitting diodes with al content graded AlGaN electron blocking layers," *IEEE Photon. J.*, vol. 5, no. 4, Aug. 2013, Art. no. 8200309.

[6] G. Verzellesi et al*et al.*, "Efficiency droop in InGaN/GaN blue light-emitting diodes: Physical mechanisms and remedies," *J. Appl. Phys.*, vol. 114, no. 7, 2013, Art. no. 071101.

[7] H. C. Zhang *et al.*, "Compositionally graded III-nitride alloys: Building blocks for efficient ultraviolet optoelectronics and power electronics," *Rep. Prog. Phys.*, vol. 84, no. 4, Mar. 2021, Art. no. 044401.

[8] Z. H. Zhang *et al.*, "A hole modulator for InGaN/GaN light-emitting diodes," *Appl. Phys. Lett.*, vol. 106, no. 6, Feb. 2015, Art. no. 063501.

[9] H. Z. Shi *et al.*, "Performance improvements of algan-based deep-ultraviolet light-emitting diodes with specifically designed irregular saw-tooth hole and electron blocking layers," *Opt. Commun.*, vol. 441, pp. 149–154, Feb. 2019.

[10] Z. J. Ren *et al.*, "Band engineering of III-nitride-based deep-ultraviolet light-emitting diodes: A review," *J. Phys. D Appl. Phys.*, vol. 53, no. 7, Dec. 2019, Art. no. 073002.

[11] C. Zhang *et al.*, "Performance improvement of algan-based deep ultraviolet light-emitting diodes with double electron blocking layers," *Chin. Phys. B.*, vol. 25, no. 2, 2016, Art. no. 028501.

[12] J. Y. Chang, H. T. Chang, Y. H. Shih, F. M. Chen, M. F. Huang, and Y. K. Kuo, "Efficient carrier confinement in deep-ultraviolet light-emitting diodes with composition-graded configuration," *IEEE Trans. Electron Devices*, vol. 64, no. 12, pp. 4980–4984, Dec. 2017.

[13] C. Chu *et al.*, "On the origin of enhanced hole injection for algan-based deep ultraviolet light-emitting diodes with AlN insertion layer in p-electron blocking layer," *Opt. Exp.*, vol. 27, no. 12, pp. A620–A628, 2019.

[14] M. Kneissl, T. Y. Seong, J. Han, and H. AmanoC, "The emergence and prospects of deep-ultraviolet light-emitting diode technologies," *Nat. Photon*, vol. 13, pp. 233–244, Apr. 2019.

[15] D. S. Wuu *et al.*, "Enhanced output power of near-ultraviolet InGaN–GaN LEDs grown on patterned sapphire substrates," *IEEE Photon. Technol. Lett.*, vol. 17, no. 2, pp. 288–290, Feb. 2005.

[16] K. Tadatomo *et al.*, "High output power InGaN ultraviolet light-emitting diodes fabricated on patterned substrates using metalorganic vapor phase epitaxy," *Jpn. J. Appl. Phys. Lett.*, vol. 40, no. 6B, pp. L583–L585, Jun. 2001.

[17] T. Mukai, K. Takekawa, and S. Nakamura, "InGaN-based blue light-emitting diodes grown on epitaxially laterally overgrown GaN substrates," *Jpn. J. Appl. Phys.*, vol. 37, pp. L839–L841, Jul. 1998.

[18] B. M. Imer, F. Wu, S. P. DenBaars, and J. S. Speck, "Improved quality (11(2) over-bar-0) a-plane GaN with sidewall lateral epitaxial overgrowth," *Appl. Phys. Lett.*, vol. 88, 2006, Art. no. 061908.

[19] H. Amano, N. Sawaki, I. Akasaki, and Y. Toyoda, "Metalorganic vapor phase epitaxial growth of a high quality GaN film using an AlN buffer layer," *Appl. Phys. Lett.*, vol. 48, no. 5, pp. 353–355, Dec. 1986.

[20] Y. L. Wang *et al.*, "Double superlattices structure for improving the performance of ultraviolet light-emitting diodes," *Chin. Phys. B.*, vol. 28, no. 3, 2019, Art. no. 038502.

[21] J. X. Wu, P. Li, X. Zhou, J. Wu, and Y. Hao, "Increasing the carrier injection efficiency of gan-based ultraviolet light-emitting diodes by double al composition gradient last quantum barrier and p-type hole supply layer," *IEEE Photon. J.*, vol. 13, no. 2, Apr. 2021, Art. no. 8200108.

[22] Z. H. Zhang *et al.*, "On the hole accelerator for III-nitride light-emitting diodes," *Appl. Phys. Lett.*, vol. 108, no. 15, 2016, Art. no. 151105.

[23] Z. T. Lin *et al.*, "Achieving high-performance blue GaN-based light-emitting diodes by energy band modification on $al_xIn_yGa_{1-x-y}N$ electron blocking layer," *IEEE Trans. Electron Devices*, vol. 64, no. 2, pp. 472–480, Feb. 2017.

[24] B. Heying *et al.*, "Role of threading dislocation structure on the x-ray diffraction peak widths in epitaxial GaN films," *Appl. Phys. Lett.*, vol. 68, no. 5, pp. 643–645, Jan. 1996.

[25] S. R. Lee *et al.*, "Effect of threading dislocations on the bragg peakwidths of GaN, AlGaN, and AlN heterolayers," *Appl. Phys. Lett.*, vol. 86, no. 24, 2005, Art. no. 241904.

[26] W. H. Sun, S. J. Chua, L. S. Wang, and X. H. Zhang, "Outgoing multiphonon resonant raman scattering and luminescence in Be- and C-implanted GaN," *J. Appl. Phys.*, vol. 91, no. 8, pp. 4917–4921, Apr. 2002.

[27] S.T. Kim, Y.J. Lee, D.C. Moon, C.H. Hong, and T. K. Yoo, "Preparation and properties of free-standing HVPE grown GaN substrates," *J. Cryst. Growth*, vol. 194, pp. 37–42, 1998.

[28] T. Jiang *et al.*, "Morphological dependent indium incorporation in InGaN/GaN multiple quantum wells structure grown on 4° misoriented sapphire substrate," *AIP Adv.*, vol. 6, no. 3, Mar. 2016, Art. no. 035316.

[29] A. V. Lobanova, A. L. Kolesnikova, A. E. Romanov, S. Yu. Karpov, M. E. Rudinsky, and E. V. Yakovlev, "Mechanism of stress relaxation in (0001) InGaN/GaN via formation of V-shaped dislocation half-loops," *Appl. Phys. Lett.*, vol. 103, no. 15, Oct. 2013, Art. no. 152106.

[30] N. H. Niu *et al.*, "Enhanced luminescence of InGaN/GaN multiple quantum wells by strain reduction," *Solid State Electron.*, vol. 51, no. 6, pp. 860–864, 2008.